MICROBIOLOGY

Autoinducing peptides regulate antibiotic production to potentially shape root microbiome

Nanzhu Chen[1]†, Peiyan Cai[1]†, Xiaoqian Lin[1]†, Zhi-Man Song[1], Jiaze He[1], Zewen Li[2], Zhuohan Li[1], Dengwei Zhang[1], Yi Song[2]*, Yong-Xin Li[1]*

Microbes use signaling molecules to regulate multiple physiological processes and mediate chemical interactions. Decoding these chemical languages is instrumental in comprehending microbial regulatory mechanisms within complex microbiota. Here, we discover previously unidentified autoinducing peptides (AIPs) derived from the plant probiotic bacterium *Paenibacillus polymyxa*, identified as Pp-AIPs. Omics analyses coupled with genetic manipulations revealed that Pp-AIP1 could effectively modulate the production of multiple antimicrobial secondary metabolites at nanomolar concentration, expanding known AIP functions. Furthermore, through inoculating *P. polymyxa* in the natural rhizosphere microbiome and analyzing its antagonistic interactions against root microbes, we suggest that Pp-AIPs may influence the microbial community composition through modulating the antimicrobial spectrum. Global analysis of biosynthetic gene clusters (BGCs) reveal widespread co-occurrence of uncharacterized AIPs with secondary metabolite BGCs. This study underscores the unreported roles of AIPs in antibiotic regulation and the microbiome interactions, advancing knowledge of quorum-sensing mechanisms in microbial ecosystems.

INTRODUCTION

Bacteria use intricate intercellular signaling mechanisms to regulate cellular behavior throughout their populations, which is known as quorum sensing (QS) (*1*, *2*). Typically, Gram-negative (G^-) bacteria mainly use small molecules referred to as autoinducers for QS (*3*, *4*), while Gram-positive (G^+) bacteria predominantly use signaling peptides (*3*, *5*). Representative QS signaling molecule families include acyl-homoserine lactone (AHL) (*6*), (2S,4S)-2-methyl-2,3,3,4-tetrahydroxytetrahydrofuran-carbonate (S-THMF-carbonate, also known as autoinducer-2, AI-2) (*7*), *N*-heterocycle (*8*, *9*), RRNPP peptide (*10*), and autoinducing peptide (AIP) (*11*) (Fig. 1A). These signaling molecules play a pivotal role in governing a myriad of physiological processes of bacteria, encompassing virulence factor production, biofilm formation, sporulation, among others (*12*, *13*). Decoding these bacterial chemical languages is crucial for unveiling the microbial physiological mechanisms, leading to the development of innovative strategies in medicine, agriculture, and industry (*14*).

AIPs are a class of cyclic thiodepsipeptide QS molecules synthesized by the accessory gene regulator (*agr*) locus in G^+ bacteria. The classic *agr* QS system comprises four main components: AgrD, the precursor peptide; AgrB, responsible for AIP processing and secretion; AgrC, a sensor kinase that detects mature AIP; and AgrA, a response regulator that governs downstream genes upon phosphorylation (Fig. 1B) (*15*). The reported AIPs have been documented to regulate virulence (*15*–*17*) and differentiation (*18*, *19*). In addition, coagulase-negative staphylococci from skin use AIPs to inhibit *Staphylococcus aureus*' *agr* QS system (*20*, *21*), mediating the bacteria-bacteria interspecies interactions. While most research has focused on AIPs in staphylococcal species (*20*, *22*), the diversity and regulatory functions of AIPs within other species and their potential roles in complex microbiome remain to be elucidated.

The root microbiome, which provides host plants with diverse microbe-derived compounds and characteristics, critically affects plant development and stress tolerance (*23*). Numerous investigations have elucidated that core microbiomes are well adapted to diverse plant roots, and the selective recruitment of particular bacterial species from the soil by plants may imply a beneficial relationship (*24*, *25*). For example, *Paenibacillus*, which produces a variety of active secondary metabolites (*26*, *27*), is a crucial component of the core microbiome in numerous agriculturally important crops and is regarded as a "plant probiotic" (*28*, *29*). However, the molecular mechanisms and chemical language for regulating its physiological behaviors and governing the microbiome remain largely unexplored.

In this study, leveraging omics analysis and bioactivity-guided discovery, we characterized a previously unidentified AIP family from *Paenibacillus polymyxa*, which unprecedently regulates antibiotic production. Moreover, our study reveals that the *P. polymyxa* can potentially shape the root microbiome of *Arabidopsis thaliana* via antagonistic interactions mediated by AIPs. To our knowledge, this study represents the first evidence of AIP's capability to regulate secondary metabolite production and its impact on microbiome composition, prompting further investigation into other potential AIPs with this function. Our comprehensive genome mining and co-occurrence analysis suggest that the largely unexplored AIPs likely regulate a variety of secondary metabolites. These findings provide valuable insights into the previously uncharacterized AIPs and underscore the ecological importance of QS autoinducers within a complex microbiome.

RESULTS

Deciphering the key signaling molecule regulating the secondary metabolites production

Genomic analysis has revealed that *Paenibacillus* contains various autoinducer genes (*30*, *31*), including the *CAR* gene for *N*-heterocycles, the *agr* locus for AIP, and the *luxS* gene for AI-2, yet their encoded

[1]Department of Chemistry, The University of Hong Kong, Pokfulam Road, Hong Kong, China. [2]Shenzhen Key Laboratory of Plant Genetic Engineering and Molecular Design, Institute of Plant and Food Science, Department of Biology, School of Life Sciences, Southern University of Science and Technology, Shenzhen, China.
*Corresponding author. Email: yxpli@hku.hk (Y.-X.L.); songy3@sustech.edu.cn (Y.S.)
†These authors contributed equally to this work.

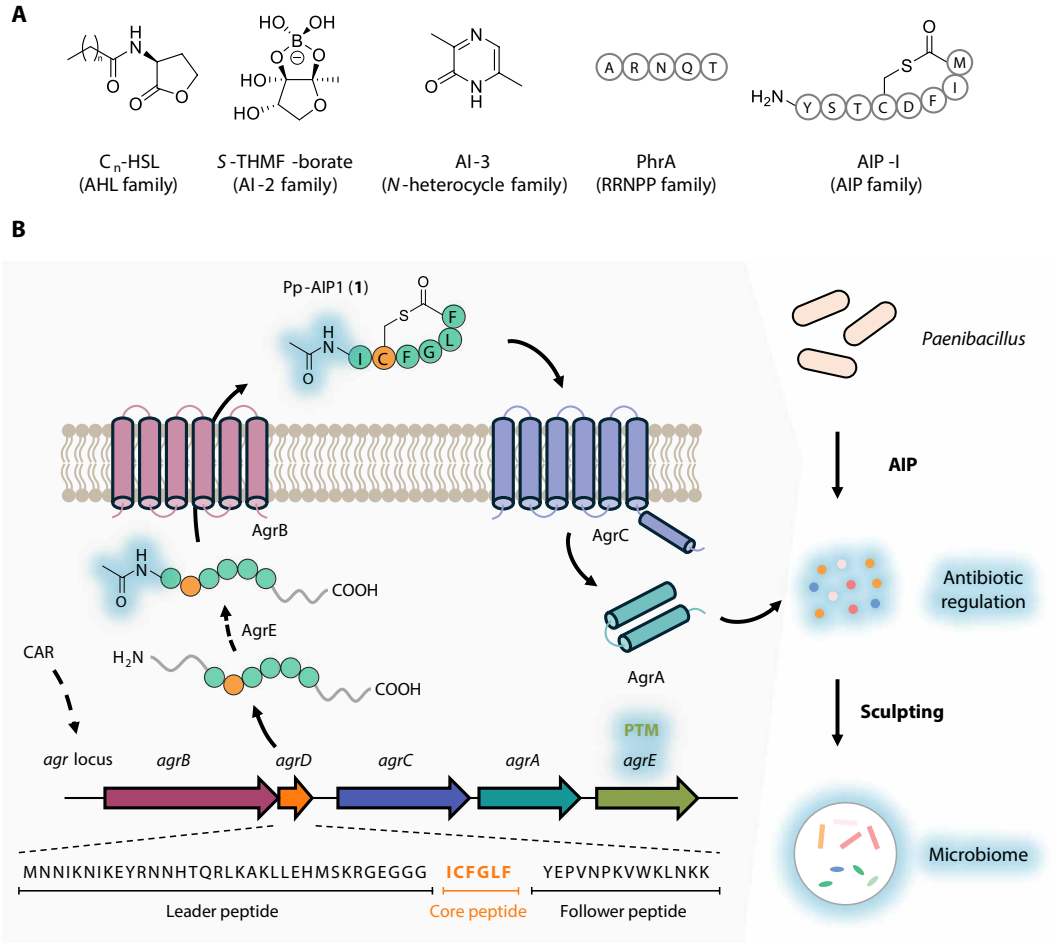

Fig. 1. An overview of AIP-mediated cross-talk discovered in this study. (**A**) Representative QS autoinducer families, including AHL, AI-2, *N*-heterocycle, RRNPP peptide, and AIP family. (**B**) The proposed illustration depicts the *agr* QS system of *P. polymyxa* reported in this study, highlighting its biosynthesis with post-modification (AgrE), roles in antibiotic regulation, and potential ecological roles in affecting microbiome. PTM, post-translational modification.

signaling molecules remain unknown, primarily due to their minimally low concentration (*9*, *20*). Our recent study demonstrated that CARs (carboxylic acid reductases) from different Bacillota species exhibited substrate tolerance and could biosynthesize an array of *N*-heterocyclic compounds (*30*), which share structural resemblances with known QS autoinducers in the *N*-heterocycle family (*8*, *9*). To study whether the CARs encode functional autoinducers, we conducted comparative omics analysis between *P. polymyxa* ATCC 842 and its Δ*CAR* mutant. The transcriptomic analysis revealed a widespread alteration in the expression of biosynthetic genes responsible for secondary metabolites in Δ*CAR* strains (fig. S1). Further, a marked decrease in various metabolites, including tridecaptin, polymyxin, paenilan, paenibacillin, and unknown compounds, was observed in Δ*CAR* (Fig. 2A). These results indicated that the *CAR* gene was involved in the global regulation of secondary metabolite production in *P. polymyxa*.

To uncover the signaling molecule involved in the regulatory process, the promoter of the paenibacillin biosynthetic gene cluster (BGC) was selected to design the reporter strain for bioassay-guided discovery. Specifically, the promoter region of the precursor gene in paenibacillin BGC (Ppae) was fused to the *lacZ* gene and introduced into the wild-type (WT) strain (*P. polymyxa*–Ppae–*lacZ*). Subsequently, the crude extracts from WT and Δ*CAR* fermentations were introduced to the reporter strain, respectively, and the lacZ activity was assessed after 16 hours (Fig. 2B). The activity result showed that the WT crude extract significantly enhanced the lacZ activity, while the Δ*CAR* crude extract did not (Fig. 2C), suggesting the presence of signaling molecules in the WT crude extract that may serve as activators.

Following this, we first examined whether the signaling molecules are the *N*-heterocycle products of CAR. Using our established method (*30*), we obtained the products of CAR through heterologous expression in *Bacillus subtilis* JH642 and introduced them to the reporter strain. However, lacZ activity was not enhanced, suggesting that the signaling molecule is regulated but not directly encoded by the *CAR* gene (fig. S2). Thus, we turned to bioassay-guided discovery of the signaling molecule (Fig. 2B). We extracted a 10-liter WT fermentation, conducted bioactivity-guided fractionation, and performed a search using the reporter strain. As a result, a peptidic compound (**1**) was identified as having Ppae-inducing activity (Fig. 2C and fig. S3). Using liquid chromatography–tandem mass spectrometry (LC-MS/MS) analysis and small-peptide gene prediction with Prodigal (*32*), we identified compound **1** as a previously unidentified AIP ($[M+H]^+$ = 723.3564, designated as Pp-AIP1), derived from a typical AIP [designated as Pp-AIP2 (**2**)] containing the amino acid sequence of ICFGLF.

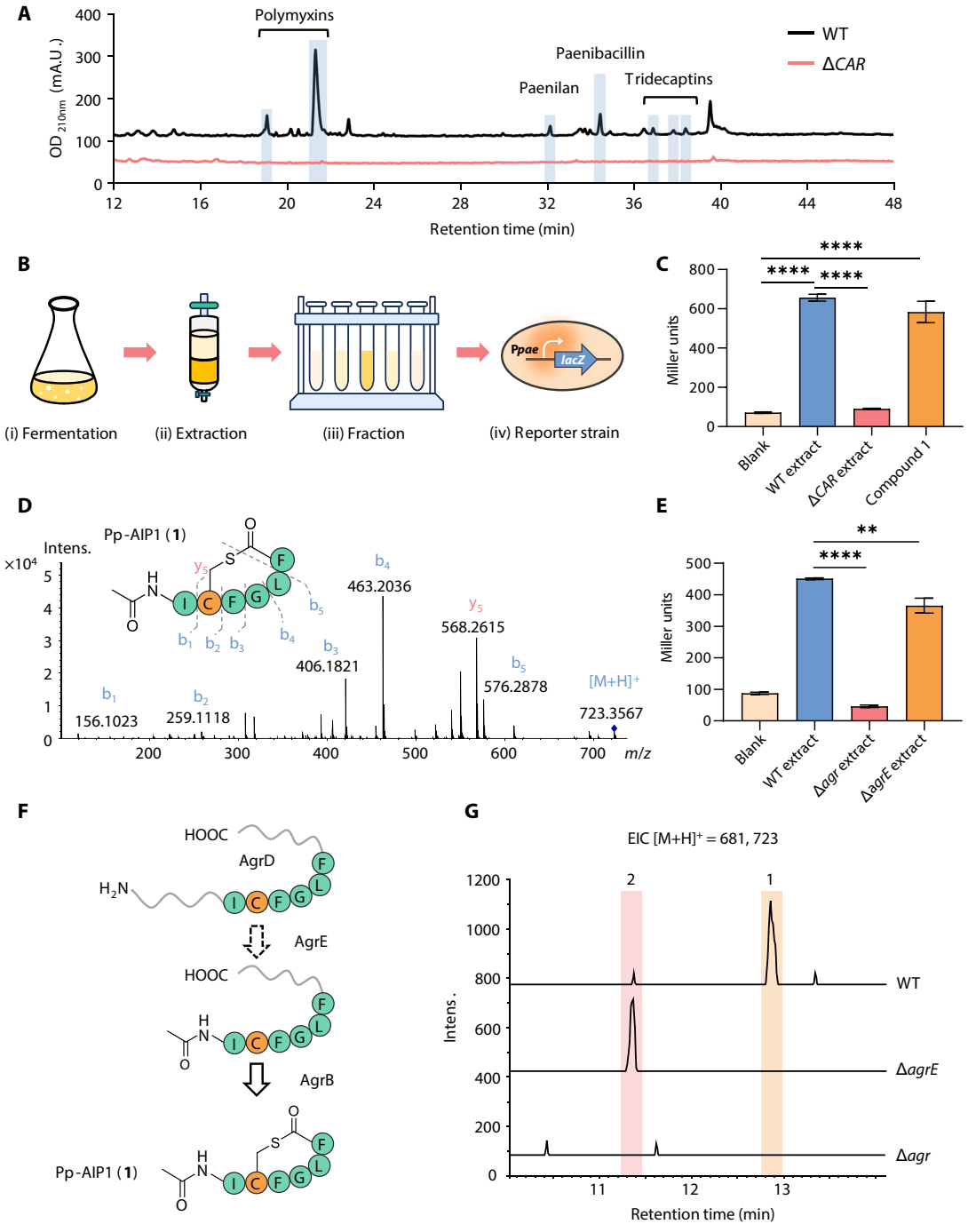

Fig. 2. Identification of signaling molecule Pp-AIPs in antibiotic regulations. (**A**) HPLC analysis of the metabolites from *P. polymyxa* ATCC 842 WT and Δ*CAR* mutant. The peaks of known products have been marked. The analysis was conducted with three independent biological replicates, and a representative result from one replicate is displayed here for clarity. mA.U., milliabsorbance unit. (**B**) The workflow of bioassay-guided identification of the signaling molecule, using *P. polymyxa*–Ppae–*lacZ* reporter assay. (**C**) The lacZ activity of reporter strain *P. polymyxa*–Ppae–*lacZ* in the presence of *P. polymyxa* ATCC 842 WT extract, Δ*CAR* extract, and compound **1**. The data are presented as mean values of three independent biological replicates ± SD (****$P < 0.0001$, unpaired two-tailed *t* test). (**D**) The MS/MS analysis of Pp-AIP1 (**1**). *m/z*, mass/charge ratio. (**E**) The lacZ activity of reporter strain in the presence of *P. polymyxa* ATCC 842 WT extract, Δ*agr* extract, and Δ*agrE* extract. The data are presented as mean values of three independent biological replicates ± SD (**$P < 0.01$; ****$P < 0.0001$, unpaired two-tailed *t* test). (**F**) Biosynthesis of Pp-AIP1 with post-modification. (**G**) EICs of Pp-AIP products (**1** and **2**) in *P. polymyxa* ATCC 842 WT, Δ*agrE*, and Δ*agr*. The analysis was conducted with three independent biological replicates, and a representative result from one replicate is displayed here for clarity. Traces are vertically offset to prevent overlap, and baseline differences do not reflect absolute signal intensities.

We identified an unprecedented modification in Pp-AIP1 (**1**), an additional acetyl group on the N-terminal of the core peptide, discovered through MS/MS fragment analysis and biosynthetically guided metabolic examination (Fig. 2D and fig. S4) (*33*). To validate the structures of Pp-AIPs, we compared natural products (**1** and **2**) with their chemically synthesized counterparts. LC-HRMS (liquid chromatography–high-resolution mass spectrometry) results showed identical retention times for both (figs. S5 and S6), and further MS/MS (figs. S4 and S7) as well as nuclear magnetic resonance (NMR) analyses (figs. S8 to S17 and tables S1 and S2) supported the proposed structures of the natural Pp-AIP1 and Pp-AIP2 products. As expected, the CAR system regulates the production of AIPs, as shown by substantial decreases in *agrB* and *agrD* gene expression and the absence of these AIPs in the metabolic profile of the Δ*CAR* strain (fig. S18). In line with the Δ*CAR* crude extract, the Δ*agr* extract also showed no inducing activity on the reporter strain (Fig. 2E), further endorsing Pp-AIPs' role as signaling molecules for secondary metabolite regulation.

Acetylation modification in AIP improves its potency

Prior studies indicate that the diversity of AIPs mainly arises from the variations of genetically encoded precursor peptides, resulting in varying levels of activity (*15*, *19*, *20*). Notably, Pp-AIP1 is the first AIP exhibiting post-modification beyond the cyclization process, warranting further exploration of its biosynthesis and functional properties. Through genomic analysis, we discovered a previously uncharacterized gene, *agrE*, adjacent to the agr locus (table S3), which may encode an acetyl transferase for Pp-AIP's acetylation (Figs. 1B and 2F). To test this, we expressed the *agrBD* and *agrBDE* genes in *B. subtilis* 168. LC-HRMS analysis confirmed that Pp-AIP1 is only observed in the presence of *agrE*, while Pp-AIP2 is produced when the *agrBD* genes are expressed (fig. S19). The *agrE* gene deletion strain failed to generate Pp-AIP1, but Pp-AIP2 production increased notably. In the *agr* deletion strain, neither Pp-AIPs were detected, further confirming the role of the *agrE* gene in Pp-AIP2 acetylation (Fig. 2G).

We next examined how acetylation influences Pp-AIPs' biological activity by subjecting extracts from *P. polymyxa* ATCC 842 WT, Δ*agrE*, and Δ*agr* to the reporter strain *P. polymyxa*–Ppae–*lacZ*. Compared to the WT extract, the Δ*agr* extract did not exhibit any inducing activity, while the Δ*agrE* extract displayed relatively lower inducing activity (Fig. 2E). Additionally, we analyzed the inducing activity of extracts from heterologous expression strains *B. subtilis* 168::*agrBD* and *B. subtilis* 168::*agrBDE*. The results showed that the extract from *agrBDE* demonstrated significantly higher activity compared to the other extracts (fig. S20). On the basis of these results and metabolic profiles, we suggest that both Pp-AIP1 and Pp-AIP2 have inducing activities, but Pp-AIP1, matured with N-terminal acetylation, is more potent.

We also conducted activity assays of synthetic Pp-AIP1 and Pp-AIP2 at various doses. LC-MS quantification showed concentrations of 24.5 nM for Pp-AIP1 and 3.7 nM for Pp-AIP2 in the WT extract (fig. S21). The inducing activity of both Pp-AIPs was then assessed at matching concentration levels (1 to 25 nM). Pp-AIP1 showed significant induction activity at just 1 nM. Although the induction activity of both Pp-AIPs increased with concentration, Pp-AIP2's activity was lower at the same concentrations (Fig. 3A). These results indicate that acetylation boosts Pp-AIP1's induction potency, suggesting that it might act as a matured signaling molecule in microbial communication.

AIPs globally regulate the production of antibacterial secondary metabolites

While previous studies primarily linked AIPs to the regulation of virulence factors (*15*) and differentiation processes (*18*) (table S4, listing reported AIPs), to our knowledge, our findings provide the first evidence that AIPs can modulate secondary metabolite expression. After confirming Pp-AIPs' stimulating impact on the paenibacillin BGC, we broadened our investigation to understand their extended influence on other BGCs. We looked at the transcription levels of BGCs in *P. polymyxa* ATCC 842 WT, Δ*agr*, and Δ*agrE*. We noticed changes in the transcription levels of most known BGCs, irrespective of their positions within the genome (Fig. 3, B and C). Inactivation of the *agr* locus had a remarkable influence, particularly on paenibacillin and paenilan of ribosomally synthesized and posttranslationally modified peptides (RiPPs) and tridecaptin and polymyxin of nonribosomal peptides (NRPs). Specifically, the *RS20960* gene in the paenibacillin BGC was down-regulated by 99.9%, and the *RS24800* gene in the paenilan BGC was up-regulated by 1.7-fold. For the Δ*agr*E strain, the effects were comparable but less intense.

In line with these transcriptional changes, we observed corresponding alterations at the metabolic level. The production of paenibacillin and tridecaptin in the Δ*agr* strain decreased by 95 and 22%, respectively, compared to the WT strain, while the production of paenilan increased by 92%. In the Δ*agrE* strain, paenibacillin production decreased by 54% compared to the WT strain (Fig. 3D). These results further imply that the absence of acetylation might reduce AIP's regulatory activity on BGCs. To further validate the regulatory role of Pp-AIPs, we generated a Δ*agrD* mutant and introduced Pp-AIP1 and Pp-AIP2 into the Δ*agrD* culture. As expected, Pp-AIP replenishment increased paenibacillin and tridecaptin production and decreased paenilan production. Introducing Pp-AIPs to Δ*agrD* slightly reduced polymyxin synthesis. However, the absence of Pp-AIPs did not significantly change polymyxin production, suggesting complex regulatory mechanisms in the bacteria.

Collectively, our findings demonstrate a previously unrecognized role of AIPs in global regulation of secondary metabolite production, representing a noteworthy advancement in our understanding of QS. These results suggest that the largely unexplored AIPs across diverse bacterial strains may have substantial potential for uncharacterized biological functions, warranting further investigation.

AIP-producing *Paenibacillus* potentially shapes the root microbiome

Given that *P. polymyxa* could favorably alter the soil microbiome (*34*), we investigated whether the AIP QS autoinducers could shape the natural rhizosphere microbiome. *A. thaliana*, a model plant species, is widely used in plant-bacteria interaction studies due to its clear genetic background and rapid life cycle (*35*). Here, we applied the WT and Δ*agr* strains of *P. polymyxa* to *A. thaliana* grown in a natural soil harvested from a tropical forest (*36*) and examined their effects on root microbiota changes (Fig. 4A). Our taxonomic profiling revealed that the root microbiome of each group was predominantly made up of the bacterial phyla Pseudomonadota, Actinomycetota, and Bacteroidota, accounting for an average of 73.36, 14.08, and 7.15% of the bacterial sequences, respectively. When we compared seedlings treated with the WT strain to those treated with the Δ*agr* strain, we found no significant changes in the relative abundances of these dominant phyla. However, we did observe a significant increase in the relatively

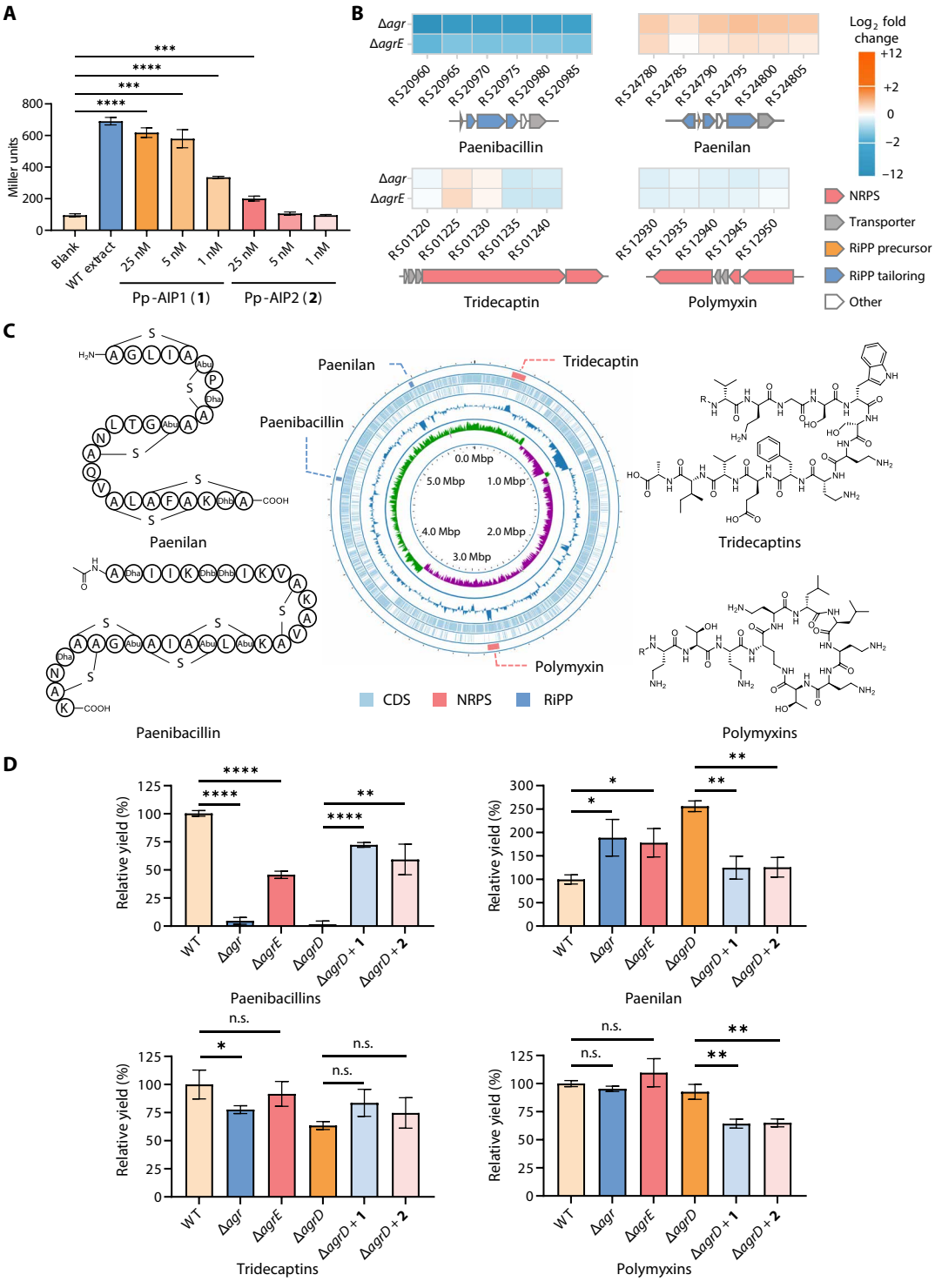

Fig. 3. Global regulation of antibiotic production by AIPs at the nanomolar scale. (**A**) The lacZ activity of reporter strain in the presence of WT strain extract and varying concentrations of synthetic Pp-AIP1 (**1**) and Pp-AIP2 (**2**). The data are presented as mean values of three independent biological replicates ± SD (***$P < 0.001$; ****$P < 0.0001$, unpaired two-tailed *t* test). (**B**) The transcription levels of identified BGCs in *P. polymyxa* Δ*agr* and Δ*agrE* strains relative to the WT strain. NRPS, nonribosomal peptide synthetase; RiPP, ribosomally synthesized and posttranslationally modified peptide. The data are presented as mean values of three independent biological replicates. (**C**) The structures of antibiotics from *P. polymyxa* ATCC 842 and the genome map display the locations of their BGCs. CDS, coding sequence. (**D**) The yield of antibiotics in WT, Δ*agr*, Δ*agrE*, Δ*agrD* strains, as well as the Δ*agrD* strain supplemented with 25 nM Pp-AIP1 or Pp-AIP2. The yield in the WT strain was calculated as 100%. The data are presented as mean values of three independent biological replicates ± SD (n.s., not significant; *$P < 0.05$; **$P < 0.01$; ****$P < 0.0001$, unpaired two-tailed *t* test).

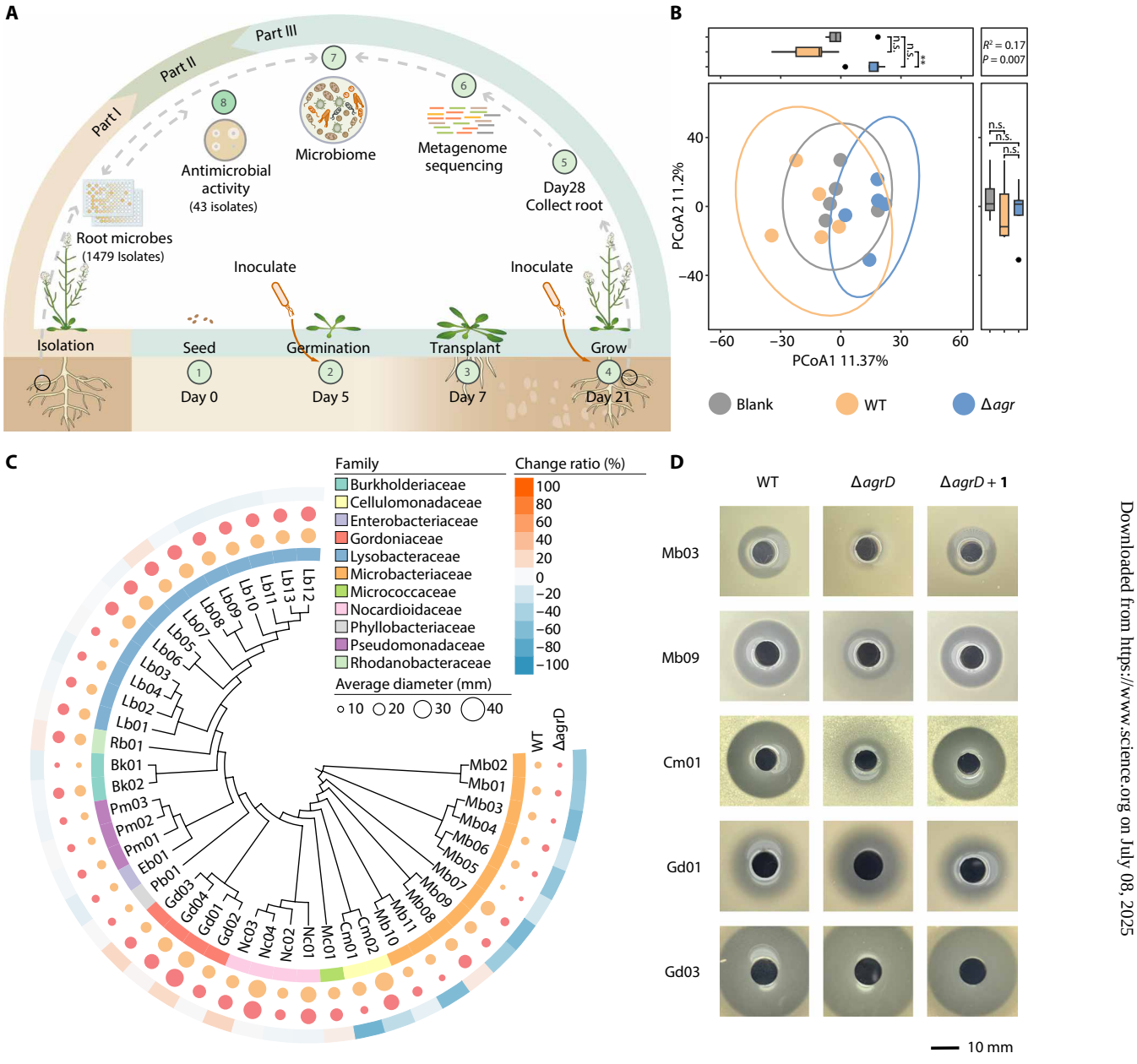

Fig. 4. Pp-AIPs shape the root microbiome via mediating antagonistic interactions. (**A**) Schematic diagram of the bacterial inoculation process on *A. thaliana*, outlining three key parts: root strain isolation, inoculation (steps 1 to 7), and antibacterial assays (step 8). (**B**) Principal coordinate analysis (PCoA) of root microbiome beta diversity in *A. thaliana* inoculated with ultrapure water (Blank), WT, and Δ*agr* strains. Ellipses show 95% confidence intervals [permutational multivariate analysis of variance (PERMANOVA) coefficient of determination (R^2) = 0.17, P = 0.007]. Box plots display variance contributions of PCoA1/2 with intergroup P values (Wilcoxon test; n.s., not significant, $^{**}P < 0.01$). Data represent five biological replicates. (**C**) The impact of *agrD* inactivation on the antibacterial activity of *P. polymyxa* against 43 bacterial isolates from the root microbiome. The orange and light red circles represent the inhibition diameter of WT or Δ*agr*. The outer sphere denotes the change ratio of the inhibition diameter (Δ*agr* versus WT). The data are presented as mean values of three independent biological replicates. (**D**) The effect of *agrD* inactivation (Δ*agrD*) and Pp-AIP1 supplementation (Δ*agrD* + **1**) on the antibacterial activity against five isolates from the root microbiome: *Microbacterium foliorum* Mb03, *M. jejuense* Mb09, *Cellulomonas humilata* Cm01, *Williamsia serinedens* Gd01, and *Gordonia soli* Gd03. The analysis was conducted with three independent biological replicates, and a representative result from one replicate is displayed here for clarity.

low-abundant but essential phyla Bacillota and Cyanobacteriota (fig. S22).

To gain further insight into the effect of treatment on root microbial diversity, we performed alpha- and beta-diversity analyses. At the species level, incubation with WT and Δ*agr* strains did not show significant changes in bacterial alpha diversity compared to the blank control (fig. S23). However, the principal coordinate analysis unveiled significant distinctions in the overall community composition between the two groups (Fig. 4B, $P < 0.01$). Specifically, the root microbiome structure colonized by the Δ*agr* strain significantly differed from that colonized by the WT strain ($P = 0.02$). Pairwise comparisons between the groups identified a total of 8.92% (787 of 8826) species with significantly different abundance between the WT and Δ*agr* groups (fig. S24). This suggests that the *agr* QS system in *P. polymyxa* could play an important role in shaping the root microbiome community.

To provide reductionist-based evidence for the regulatory impact of *P. polymyxa*'s antimicrobial activity on root microbiome changes, we tried to match the differentially abundant species with our 1479 previously isolated strains from the same natural soil (*36*). However, the limited cultivability of soil microbes prevented direct alignment. To address this, we prioritized 43 strains that were phylogenetically close to the differentially abundant species (table S5 and data S1) for experimental validation, evaluating the antimicrobial bioactivity of culture supernatant from WT, Δ*agrD*, and Δ*agrD* supplemented with Pp-AIP1. The bioactivity result showed that, in comparison to the WT, inactivation of *agrD* exhibited considerably reduced inhibition activity on most isolates from the families Microbacteriaceae and Cellulomonadaceae while showing enhanced inhibition activity against certain isolates from the families Gordoniaceae and Nocardioidaceae (Fig. 4C). Conversely, the Pp-AIP1 complementation displayed restored inhibition activity (Fig. 4D and fig. S25). Inhibition activity of purified paenibacillin and paenilan was further validated against representative isolates from these four families (fig. S26). While paenibacillin exhibited more potent inhibition activity on isolates from Microbacteriaceae and Cellulomonadaceae, the paenilan only shows higher activity on Gd01 from Gordoniaceae. These findings suggest that the altered inhibition profile of Δ*agrD* on the some soil isolates may result from differential production of paenibacillin and paenilan.

Overall, these results demonstrated that the presence of the *agr* system in *P. polymyxa* finely alters the antimicrobial spectrum via Pp-AIPs and selectively influences specific genera within the root microbiome. These interactions could contribute to observable shifts in rhizosphere community composition, although further validation is required to resolve whether these effects are direct or context dependent. As the ecological functions of AIPs within complex microbial ecosystems remain underexplored, our findings provide mechanistic insights into QS-mediated interactions in natural microbiome.

The prevalent and diverse AIPs coexist with other BGCs in bacteria

Despite the significance of AIPs in bacterial physiology, over more than 20 years, only 43 AIPs have been identified across six species (table S4). Given our discovery of AIPs with regulatory function, we aim to expand the exploration of uncharacterized AIPs and identify potential AIPs with similar function. To show the current state of AIP discovery and to offer insights for future studies, we conducted a systematic genome mining analysis of *agr* BGCs (Fig. 5A). Initially, we used antiSMASH 6.1.1 to investigate genes encoding AgrB enzymes across 223,243 bacterial genomes within the RefSeq genomes, which resulted in 40,850 hits (data S2 and S3). We then identified 29,921 AgrD precursor peptide sequences (data S4). To overcome the limitations of antiSMASH in identifying certain AIP precursor peptides, we used TrRipp (*37*) to mine RiPP precursors, generating an additional 4704 precursor peptide sequences (data S4).

The vast majority of the predicted AgrD sequences, more than 99.9%, originated from the phylum Bacillota. Within Bacillota, 73.41% (26,156) of the precursors were found in the class Bacilli, and 12.83% (4,704) were from the class Clostridia (Fig. 5B). Notably, among the class Bacilli, 97.78% of the members within the family Staphylococcaceae encoded the *agrD* gene, making this family the dominant source of AIPs. The family Listeriaceae also had a high potential, with 99.19% of its members contributing a total of 4413 AgrD sequences. In the class Clostridia, Clostridiaceae contributed the most AgrD, followed by Peptostreptococcaceae and Lachnospiraceae. The widespread distribution of the AgrD across the phylum Bacillota, with particularly high prevalence in the classes Bacilli and Clostridia, underscores the potential significance of this QS system in the ecology, communication, and virulence of these medically important bacterial groups. Next, using the Enzyme Function Initiative–Enzyme Similarity Tool (EFI-EST), we analyzed AIP's diversity via sequence similarity network (SSN) analysis of AgrD sequences (fig. S27). Most known AIPs, especially from *Staphylococcus*, belonged to the largest family. Most identified AIPs do not group with any known ones, implying the underexplored status of AIPs.

To investigate the regulatory potential of AIPs in secondary metabolite production, we conducted a co-occurrence analysis of AIP precursor genes (*agrD*) with other BGCs at the genomic level. This analysis uncovered the potential association between a number of AIP families and distinct secondary metabolites, including RiPPs, NRPs, polyketides, and terpenes (Fig. 5C and data S5). Notably, AIPs showed a comparatively higher co-occurrence with secondary metabolite BGCs in the genomes of Bacillaceae and Paenibacillaceae (Fig. 5C, the clusters marked within purple dashed box). These clusters encompass several key antibiotics, including gramicidin (*38*), lichenysin (*39*), fusaricidin (*40*), paenibacillin (*41*), paenilan (*42*), and tridecaptin (*43*), along with a number of unidentified compounds. In contrast, the well-characterized AIPs from *S. aureus* (AIP-I/II/III/IV) (*15*) do not exhibit strong co-occurrence with any BGCs, which is consistent with the established notion that these AIPs primarily regulate virulence (*15*) rather than secondary metabolite production. This analysis also provides fresh insights into the function of known AIPs. For instance, while Slu-AIP, an AIP produced by *Staphylococcus lugdunensis*, is known to inhibit the *agr* system in *S. aureus* (*44*), its function in the native host remains uncharacterized. Our co-occurrence analysis implies a potential association between Slu-AIP and lugdunin (*45*), a potent antibiotic against *S. aureus*, suggesting that Slu-AIP may play multiple roles in the interspecies interactions with *S. aureus*.

In conclusion, the co-occurrence patterns of AIP-BGC observed in our analysis suggest a statistically notable association (co-occurrence rate > 50%) between AIPs and BGCs for active secondary metabolites across diverse species, particularly within the Bacillaceae and Paenibacillaceae. While these findings highlight the considerable diversity of uncharacterized AIPs and their potential ecological roles in microbiome modulation, we emphasize that physical co-localization does not necessarily imply regulatory control, as evidenced by the selective

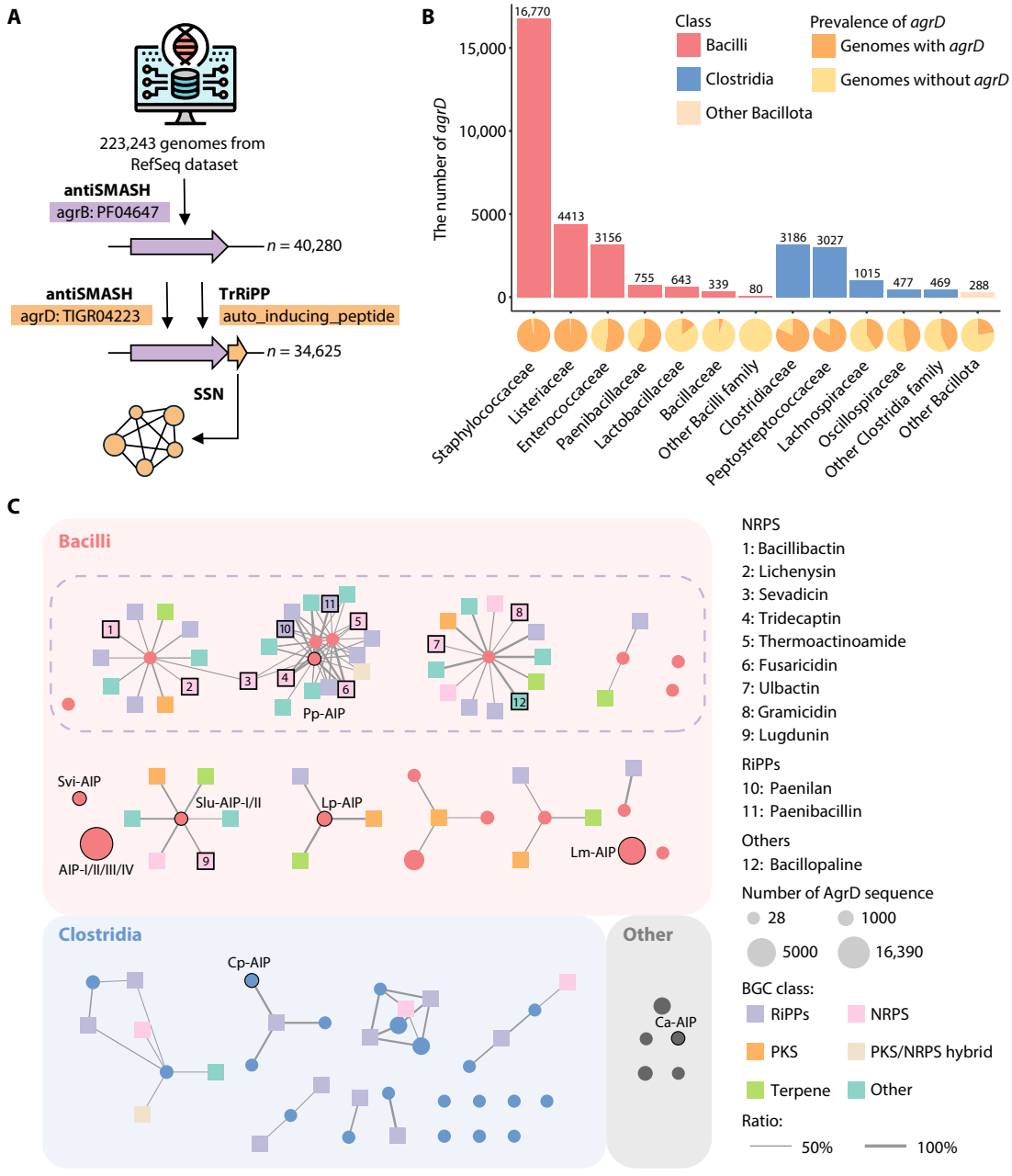

Fig. 5. The diversity and prevalence of AIPs and their co-occurrence with other metabolites. (**A**) Overview of the mining workflow of *agr* BGCs. (**B**) The distribution of *agrD* in Bacillota. The *x* axis represents the family of origin genome, with colors indicating different classes. The pie chart illustrates the prevalence of *agrD* within the genomes of each corresponding family. (**C**) Co-occurrence network of *agrD* family and BGC cluster. Relationships with co-occurrence rates > 50% are shown in the figure, and the thickness of the edge represents the co-occurrence rate. Circles represent families containing more than 25 *agrD* sequences, with their size proportional to the number of sequences. Reported AIPs are marked with a black border. Squares denote BGC clusters, colored according to their type, with known BGCs labeled by numbers. The *agrD* and BGCs from Bacillaceae and Paenibacillaceae are marked within purple dashed box.

effects of Pp-AIP1 on specific metabolites in this study. The genome mining data presented here provide a valuable framework for future experimental validation of AIP-BGC interactions.

DISCUSSION

Understanding the complex "language" of cellular chemicals in microbes and their role in biological functions has long been a key focus in microbiology and chemical biology. AIPs have attracted research attention due to their wide distribution (*46*) and strong association with virulence factors (*15*). However, their diversity, in vivo functions, and ecological function within complex environment remain largely unexplored. In this study, using bioactivity-guided screening and genomic analysis, we identified Pp-AIPs from *P. polymyxa*, which are responsible for globally regulating antibiotic production. Furthermore, by conducting multi-omics analysis and systematic

biosynthetic analysis, we notably widened the chemical landscape of AIPs and unveiled their concealed roles in secondary metabolite regulation. The co-occurrence analysis of the *agrD* with the other BGCs suggests that AIPs may have a wide-ranging impact on diverse secondary metabolites. These findings offer valuable insights into the functional diversity of AIPs, intensifying interest in their vital roles in a variety of bacterial physiological processes.

Researchers have been captivated by the variety in AIP structures and their prominent signaling roles. Gless *et al.* (*20*, *22*), using a native chemical ligation method, identified a variety of AIPs exhibiting differential QS inhibitory activity against *S. aureus*, attributed to amino acid variations in thiodepsipeptides. Recent studies suggest some AIPs transform from thiodepeptides to homodetic cyclopeptides via an *S*-acyl–to–*N*-acyl shift, significantly altering their activities (*47*). Here, we present an acetylated AIP, an unreported case with acetylation post-modification, which enhances bioactivity and enables efficiently control of the production of multiple antimicrobial secondary metabolites at nanomolar concentrations. Even so, the genome mining and SSN analysis of AIPs revealed that most of identified AIPs only represent very limited family, suggesting the substantial structural diversity within unexplored AIPs.

The discovered AIPs have been reported to regulate virulence (*15*, *17*) and differentiation (*18*, *19*). In this study, we found that Pp-AIPs significantly regulate the production of paenilan and paenibacillin with remarkable potency against G^+ bacteria (*41*, *42*), as well as affect the production of tridecaptins and polymyxins targeting G^- bacteria. Meanwhile, the co-occurrence analysis of AIPs and BGCs suggests that this phenomenon may not be an isolated incident and indicates a widespread association between AIPs and BGCs for secondary metabolites in specific bacterial families. Moreover, we observed a positive correlation between the existence of *CAR* gene and the expression levels of *agr* locus as well as a series of BGCs in *P. polymyxa*. Nevertheless, the regulation mechanism and process by which *CAR* gene globally manages secondary metabolite production remain unknown.

Given the important role of antibiotics in microbial interaction, extensive efforts have been made to investigate their regulation mediated via QS autoinducers. For instance, C6-HSL has been shown to stimulate the production of the antibiotic phenazine-1-carboxamide in *Pseudomonas chlororaphis* (*48*), while ComX pheromone is reported to regulate surfactin synthesis in *B. subtilis* (*49*, *50*). Similarly, valdiazen is found to modulate fragin production in *Burkholderia cenocepacia* (*51*). Collectively, these studies highlight the diversity of bacterial QS systems in regulating antibiotic synthesis. This regulatory plasticity may confer ecological advantages to microbes through targeted inhibition of competitors or modulation of community architectures. In this study, the discovery of Pp-AIPs uncovers a previously unrecognized antibiotic regulatory mechanism mediated by AIPs, a class of autoinducers widely existing in G^+ bacteria, offering fresh insights into microbial antibiotic expression and interspecies antagonism.

Known as intraspecies QS autoinducers, AIPs are now attracting interest for their involvement in interspecies interactions. Emerging evidence from recent investigations has demonstrated that AIPs derived from coagulase-negative Staphylococcal strains exhibit inhibitory effects on the *S. aureus agr* QS system, thereby impeding *S. aureus* colonization within skin microbiota and attenuating the progression of cutaneous infections (*20*, *21*). While the dual-strain interactions through AIPs have been documented, the current challenge lies in understanding their influence on complex microbiota. Our investigation shows AIP-producing *Paenibacillus* exert different inhibitory effects on different microorganism families within root microbial populations. This implies that AIPs might help host bacteria adapt to diverse environments by precisely regulating antimicrobial secondary metabolites for antagonistic interactions, thereby potentially shaping microbiota structure. However, although we have observed that the existence of *agr* system in the *P. polymyxa* affects certain genus of bacteria, the ecological roles of these influenced root microbes require further exploration.

In conclusion, our research has uncovered an AIP family that can remarkably influence antibiotic production, thereby shaping the microbiota. Given the widespread presence of AIPs in different bacteria and microbiota, our study indicates that they may contribute to shaping the microbiota through the regulation of antagonistic interaction. However, the precise mechanisms through which AIPs respond to and affect microbiota balance remain to be fully elucidated, and their influence on the host needs further confirmation. We anticipate that our findings will prompt more research into the intricate interplay among QS autoinducers, the microbiota, and hosts, potentially offering benefits to areas such as human health, agriculture, and various industrial sectors.

MATERIALS AND METHODS

Strains and culture conditions

All strains used in this study are listed in table S6. *Escherichia coli* strain Trans5α, used for constructing and propagating the plasmid, was cultivated in Luria-Bertani (LB) medium [yeast extract (5 g/liter), tryptone (10 g/liter), and NaCl (10 g/liter)] at 37°C. When the *E. coli* strains contained the pJOE8999 or its derived plasmids, kanamycin (50 μg/ml) was supplemented to the medium. When the *E. coli* strains contained the pDR111 or its derived plasmids, ampicillin (100 μg/ml) was supplemented to the medium.

P. polymyxa ATCC 842 and its derived mutants were cultured in tryptic soy broth (TSB) (catalog no. 22092, Sigma-Aldrich, USA) medium at 30°C. When the *P. polymyxa* strains contained the pJOE8999 or its derived plasmids, kanamycin (35 μg/ml) was supplemented to the medium. *B. subtilis* 168 and derived heterologous expression strains were cultured in LB medium at 30°C.

HPLC metabolic profile analysis of *P. polymyxa*

For metabolic profiles analysis of the *P. polymyxa* strains, the *P. polymyxa* ATCC 842 WT and mutant strains were cultured overnight as seed culture and, subsequently, inoculated into 20 ml of glucose-starch-$CaCO_3$ (GSC) medium (*52*) at a ratio of 1:40 (v/v). After 2 days of liquid culture at 30°C and 200 rpm (Φ 26 mm), the fermentation samples were collected. Each sample was mixed with an equal volume of methanol (MeOH). After vortex, centrifuge (12,000*g* for 10 min), and filter (0.22 μm), the samples were then analyzed using 1525 BINARY high-performance liquid chromatography (HPLC) system (Waters, USA) equipped with an XB-C18 analysis column (5 μm, 100 Å, 250 mm by 4.6 mm) (Phenomenex, USA). The gradient elution LC method uses H_2O (with 0.05% trifluoroacetic acid) as solvent A and acetonitrile (with 0.05% trifluoroacetic acid) as solvent B. The samples were eluted using a flow rate of 1 ml/min, with 15% B for 5 min, followed by 15% to 50% B for 45 min, 100% B for 5 min, and lastly 15% B for 5 min. The metabolic profile was assessed at a wavelength of 210 nm. For each experimental group, three biological replicates were conducted.

Construction of the promoter-reporter system in *P. polymyxa*

Plasmid pJOE8999-Ppae-*lacZ* was constructed for evaluating the transcription level of the paenibacillin precursor gene. The promoter region of the paenibacillin precursor was amplified with the primer pair Ppae-F/R from *P. polymyxa* ATCC 842 genome (ref. genome NZ_CP024795). The *lacZ* reporter gene was amplified with the primer pair lacZ-F/R from *E. coli* Trans5α. The linearized vector was amplified with the primer pair pJOE8999-F/R using plasmid pJOE8999 as the template. DNA fragments were assembled into the expression plasmid using the HiFi DNA Assembly Kit (catalog no. E2621, New England Biolabs, USA). Plasmids and primers used for promoter-reporter system in *P. polymyxa* ATCC 842 are detailed in tables S7 and S8.

Consequently, the plasmid pJOE8999-Ppae-*lacZ* was transformed into *P. polymyxa* ATCC 842. For transformation of plasmids into *P. polymyxa*, the overnight culture of *P. polymyxa* ATCC 842 in TSB-sorbitol (TSBS) medium (TSB with the addition of 0.5 M sorbitol) was inoculate into fresh TSBS culture medium at a ratio of 1:25 (v/v) and grow at 37°C and 200 rpm (Φ 26 mm) until the cell density reached an optical density at 600 nm (OD_{600}) of 0.5 to 0.6. The cultures were cooled with ice for 30 min and harvested by centrifugation at 6500*g* for 5 min at 4°C. The cells were washed three times with electroporation buffer (250 mM sucrose, 1 mM $MgCl_2$, 1 mM Hepes, and 10% glycerol) and resuspended in the electroporation buffer. The competent cells (50 μl) were incubated with 2 μg of plasmid on ice for 20 min and shocked with a 1.8-kV voltage using Eppendorf Eporator (Eppendorf SE, Germany). Next, the cells were mixed with 1 ml of recovery medium (TSBS) and incubated at 37°C for 3 hours. Following this incubation period, the cells were plated on selective TSB agar plates [TSB agar with kanamycin (35 μg/ml)].

β-Galactosidase activity assay

The reporter strain *P. polymyxa* ATCC 842 Ppae-*lacZ* was cultured in 5 ml of TSB medium containing kanamycin (35 μg/ml). Different samples, such as crude extracts from *P. polymyxa* WT/mutants, crude extracts from *B. subtilis* heterologous expression strains, fractions from *P. polymyxa* WT crude extracts, and synthesized AIP molecules, were added to the culture, respectively. The culturing was carried out at 30°C and 200 rpm (Φ26 mm) for 16 hours. Subsequently, 0.5 ml of each culture was collected and centrifuged at 6000 rpm for 10 min at 4°C. The cell pellets were then collected and resuspended in 0.5 ml of Z-buffer [0.06 M $Na_2HPO_4{\cdot}7H_2O$, 0.04 M $NaH_2PO_4{\cdot}H_2O$, 0.01 M KCl, 0.001 M $MgSO_4$, and 2.7% β-mercaptoethanol (pH 7.0)]. For each sample, 0.2 ml of the sample was extracted to quantify the OD_{600}. Additionally, 0.1 ml of each sample was diluted 10 times with Z-buffer and mixed with 50 μl of chloroform and 25 μl of 0.1% SDS solution. The mixture was then vortexed and incubated at 30°C for 5 min. Next, 100 μl of *o*-nitrophenyl-β-D-galactopyraniside (4 mg/ml) (catalog no. N109040, Aladdin, China) was added to each mixture to initiate the reaction. After incubating at 30°C for 15 to 20 min, 250 μl of 1 M Na_2CO_3 solution was added to stop the reaction. The samples were then vortexed and centrifuged, and the supernatant was collected for measurement of OD_{420} and OD_{550}. The lacZ activity was evaluated by the formula: Miller units = $1000 \times [(OD_{420} - 1.75 \times OD_{550})]/[\text{time (min)} \times \text{volume (ml)} \times OD_{600}]$. In each individual figure, all samples were cultured and analyzed within the same batch, and the culture extracts were collected from the same batch of fermentation under same extraction processes.

Screening for the signal molecule regulating secondary metabolites production in *P. polymyxa*

P. polymyxa ATCC 842 was fermented in GSC culture medium (10 liters) as described in HPLC metabolic profile analysis section. The culture was extracted using ethyl acetate (EA), dried, and then partitioned via a reversed-phase C18 silica gel open column with a gradient elution of MeOH and H_2O (0% to 100% MeOH). Each fraction was tested for bioactivity using the promoter-reporter system. The fraction demonstrating the most bioactivity, which was eluted with 80% MeOH, was further partitioned on a Sephadex LH20 open column using MeOH, yielding 136 fractions, which were subsequently dried. Fractions were combined in groups of 5 to 10 for initial bioactivity screening. The most bioactive fractions (LH20 fractions 30 to 35 and 35 to 40) were individually analyzed using the promoter-reporter system. Among these, the fraction with the highest bioactivity (fraction 34) was further analyzed by HPLC on a Luna C18 semi-preparative column. The gradient elution was performed with a flow rate of 2.5 ml/min, from 35% to 65% ACN/H_2O containing 0.1% trifluoroacetic acid over 50 min. Fractions were collected every 5 min, dried, and tested for bioactivity. Within the most bioactive 5-min fraction, additional fractions were collected every 30 s, dried, and tested for bioactivity. The most bioactive fraction, which contained a single peak, was subjected to LC-MS/MS analysis. For each experimental group, three biological replicates were conducted. In each individual Figure, all samples were cultured and analyzed within the same batch, and the culture extracts were collected from the same batch of fermentation under same extraction processes.

UPLC-MS/MS and NMR analytical procedures

The UHPLC-MS/MS (ultrahigh-performance liquid chromatography–tandem mass spectrometry) analyses were performed on UltiMate 3000 UHPLC system (Thermo Fisher Scientific, USA) coupled with impact II Mass Spectrometer (Bruker, Germany), equipped with the ACQUITY UPLC BEH C18 column (1.7 μm, 130 Å, 2.1 mm by 150 mm) (Waters, USA). The gradient elution LC method uses H_2O (with 0.1% formic acid) as solvent A and acetonitrile (with 0.1% formic acid) as solvent B. The samples were eluted using a flow rate of 0.2 ml/min, with 5% B for 2 min, followed by 5 to 95% B for 15 min and 95% B for 4 min, and, lastly, 5% B for 1 min. All the samples were analyzed using electrospray ionization mass spectrometry under positive ion mode with mass/charge ratio range from 150 to 1500, at data-dependent acquisition mode. The instrument's parameters were set as follows: Nitrogen was used as drying gas (8.0 liters/min, 200°C), nebulizer at 1.8 bar, capillary at 4500 V, end plate offset at 500 V. Calibration of the mass spectrometer was performed using a sodium formate standard. All LC-MS/MS data were analyzed using the software Bruker Compass DataAnalysis 4.3.

The one-dimensional (1D) and 2D NMR spectra were recorded at 298 K on an Avance DRX 600 FT-NMR spectrometer (Bruker, Germany) (600 and 150 MHz for ^1H and ^{13}C NMR, respectively), using DMSO-d_6 as solvent. The NMR data were analyzed by Mnova NMR Software (*53*).

Genetic manipulation in *P. polymyxa*

Plasmids and primers used for genetic manipulation in *P. polymyxa* ATCC 842 are detailed in tables S7 and S8. Specifically, pJOE8999-*agr*, pJOE8999-*agrE*, and pJOE8999-*agrD* were constructed to delete corresponding locus or genes in native host *P. polymyxa* using

the CRISPR-Cas9 system. The construction of these plasmids follows the protocol in Altenbuchner's work (*54*).

The corresponding plasmids for genetic deletion were transformed into *P. polymyxa* ATCC 842 following the previously described protocol, respectively. The positive transformants verified by colony PCR were cultured in TSB with kanamycin (35 μg/ml) and mannose (20 mg/ml) at 30°C to induce the expression of Cas9 for 2 days. The Cas9-induced cultures were then streaked onto fresh TSB-Agar plates and screened for positive colonies by verification PCR. For plasmid curing, the positive clones would be streaked onto TSB plates without kanamycin and incubated at 37°C.

Heterologous expression of the *agr* BGC

Plasmids and primers used for heterologous expression of the agr BGC are detailed in tables S7 and S8. Plasmids pDR111-*agrBD* and pDR111-*agrBDE* were constructed for integrated target genes into the genome of the heterologous expression host *B. subtilis* 168. The genes *agrBD* and *agrE* were amplified from *P. polymyxa* ATCC 842 genome, while the linearized vector was amplified using plasmid pDR111 as the template. The expression plasmids were assembled using DNA fragments assembly kit.

The relevant plasmids were transformed to *B. subtilis* 168 by the natural competence transformation method (*55*). The recombinant strains were cultured in LB with addition of spectinomycin (100 μg/ml) and 0.5 μM isopropyl-β-D-thiogalactopyranoside at 30°C and 200 rpm (Φ 26 mm) for 1 day. The compounds were extracted by adding an equal volume of EA. Dried EA extracts were dissolved in MeOH and analyzed by UPLC-MS/MS.

Chemical synthesis of AIP molecules

The chemical synthesis of AIPs was conducted by Nanjing Yuanpeptide Biotechnology Company (China), following the method in previously published work (*56*). Briefly, peptide synthesis was performed using an automated synthesizer with standard 9-fluorenyl methoxycarbonyl solid-phase peptide synthesis chemistry. Following peptide assembly, *N*-acyl-benzimidazolinone formation was conducted on resin using 4-nitrophenyl chloroformate, followed by cyclization and cleavage using a trifluoroacetic acid cleavage cocktail. The final cyclic peptide was purified by preparative HPLC and lyophilized to yield the desired AIP products.

Quantification of the Pp-AIP natural product

A standard curve was established to quantify the concentration of Pp-AIPs. Standard solutions of chemically synthesized Pp-AIP1 and Pp-AIP2 were prepared at concentrations of 1, 5, 12.5, 25, 50, and 100 nM, respectively. Each standard solution (2 μl) was injected into the ACQUITY H-Class UPLC system (Waters, USA) coupled with an ACQUITY SQ Detector 2 mass spectrometer (Waters, USA), equipped with the ACQUITY Premier Peptide BEH C18 column (1.7 μm, 300 Å, 2.1 mm by 150 mm) (Waters, USA), and a standard curve was generated on the basis of the peak area of the target compounds.

For determining the concentration of Pp-AIPs in its host *P. polymyxa*, 500 μl of the WT liquid culture was extracted with EA, followed by centrifugation and evaporation to dryness. The residue was dissolved in 500 μl of MeOH, and 2 μl of the sample was injected into the UPLC-MS system. The concentration of the natural product Pp-AIPs was determined by comparing their peak area with the standard curve.

Transcriptome analysis

Total RNA was extracted from 12-hour cultures. After ribosomal RNA (rRNA) removal and cDNA synthesis, paired-end 150–base pair (bp) sequencing was performed using the NovaSeq 6000 platform (Illumina, USA), yielding an average of 9,433,573 raw sequence reads per sample. Raw sequencing reads were quality controlled by fastp v0.23.2 (*57*) with parameters "--detect_adapter_for_pe -l 50 -5 3 -3 3," including removal of adapter and low-quality reads. Clean reads were then mapped to the reference genome of *P. polymyxa* ATCC 842 [National Center for Biotechnology Information (NCBI) accession number NZ_CP024795] using Bowtie2 v2.2.3 (*58*) with default parameters. FeatureCounts (*59*) was used to compute mapped reads, with parameters "-p -B -C --fracOverlap 0.2." Transcripts per million were adopted for quantifying the gene expression level, with normalizing for sequencing depth and gene length. For each experimental group, three biological replicates were conducted.

A. thaliana inoculation experiment with bacterial cultures

The bacterial inoculation experiment and sample collection were performed according to Song and co-workers' work (*36*) with modifications. In brief, surface-sterilized *A. thaliana* Col-0 seeds (using chlorine gas generated from 100 ml of bleach and 5 ml of concentrated hydrochloric acid) were sown on $^1/_2$ Morishige and Skoog (MS) medium containing 1.2% agar and 1% sucrose. Subsequently, 5-day-old seedlings were root-inoculated with 2 μl of bacterial culture (OD_{600} of 0.005) from either *P. polymyxa* ATCC 842 (WT group) or its derivative mutant generated via *agr* locus deletion (Δ*agr* group), with ultrapure water as the blank control (Blank group). After 2 days of cocultivation on plates, plants were transferred to soil. Fourteen days later, a secondary inoculation was performed by applying 5 ml of corresponding bacterial culture (OD_{600} of 0.2) or water control to the root zone. Subsequent to an additional week of growth, root samples were collected for metagenome sequencing to evaluate the organization of the root microbiome. For each experimental group, five biological replicates were conducted.

Metagenome sequencing and analysis

DNA was extracted from the collected root samples, and paired-end 150-bp sequencing was performed using the DNBSEQ-T7 platform (MGI Tech, China), yielding an average of 75,050,815 raw sequence reads per sample. Adapter sequences were removed, and the raw sequence reads were quality filtered using fastp v0.23.2 (*57*). Host sequences were removed by mapping the *A. thaliana* genome TAIR10.1 (GCF_000001735.4) using bowtie2 v2.2.3 (*58*).

The cleaned reads were taxonomically profiled using the Kraken2 v2.0.7 (*60*) pipeline. Specifically, the reads were mapped to the Kraken database (k2_standard_20240112), and the Bracken v2.9 (*61*) was used to estimate the relative abundances of taxa at different taxonomic levels. Relative abundance in a sample was defined as the number of assigned reads compared to the total number of bacterial reads.

To assess the alpha and beta diversity of the root microbiome, the R package "vegan" was used. The Wilcoxon test was used to statistically compare the abundances of specific taxa between the groups.

Root microbe isolation and inhibition assay

The 1479 root-associated microbes were isolated from *A. thaliana* Col-0 grown in natural soils collected from Xishuangbanna Tropical Botanical Garden (E101°27′, N21°92′) and Yuanjiang Savanna

Ecological Station (E102°10′, N23°28′), following previously described methods (*62*). Briefly, surface-sterilized *A. thaliana* Col-0 seeds were germinated on $^1/_2$ MS agar medium and transplanted into collected soils. After 28 days of growth, roots were harvested, washed with sterile PBS (0.1 M), sectioned into 2-mm fragments, and homogenized in 10 mM $MgCl_2$. Microbial isolation was achieved through serial dilution in R2A, 10% TSB, and ISP (international streptomyces liquid) medium.

A total of 43 isolates were acquired that were phylogenetically related to differentially abundant taxa for antimicrobial activity testing. Their 16*S* rRNA gene sequences were amplified using general primers 27F and 1492R, followed by Sanger sequencing with primer 27F. Detailed information regarding the 16*S* rRNA gene sequences, culture medium, and top-hit taxon data of these isolates can be found in data S1. The 16*S* rRNA gene sequences were aligned using MAFFT v7.490 (*63*), the results were trimmed using trimAl v1.4 (*64*), and, lastly, the tree was constructed using FastTree v 2.1.11 (*65*). iTOL (*66*) was used to visualize the phylogenetic tree.

The inhibition assay was conducted to evaluate the antimicrobial activity of culture supernatant of *P. polymyxa* ATCC 842 WT, Δ*agrD*, and Δ*agrD* supplementary with 25 nM of Pp-AIP1 against the root-associated isolates. In brief, the isolates were cultured for 1 to 3 days and diluted to OD_{600} of 0.01 into corresponding agar medium at ~45°C. Sterile Oxford cups with an external diameter of 8 mm were applied to generate uniform wells within the agar. Following this, 100 μl of supernatant of each sample was dispensed to the wells. For purified metabolite assays, paenilan and paenibacillin were extracted from fermentation liquid using HP-20 resin (catalog no. 13606, Sigma-Aldrich, USA), followed by purification on XB-C18 semi-preparation column (5 μm, 100 Å, 250 mm by 10 mm) (Phenomenex, USA). Aliquots (100 μl of fermentation liquid equivalents) of purified metabolites were then dispensed into wells for inhibition zone analysis. The plates were then incubated at 30°C for 24 to 48 hours, and the diameters of the inhibition zones around each cup were measured in millimeters to assess antimicrobial efficacy. For each experimental group, three biological replicates were conducted. In each figure, the samples for assay were cultured within the same batch and extracted under consistent processes.

Genome mining of *agr* BGC and co-occurrence analysis

In this study, a comprehensive analysis was conducted on a dataset of 223,243 bacterial genomes obtained from the NCBI RefSeq database. The genomes were subjected to antiSMASH 6.1.1 (*67*), a widely used BGCs mining tool.

To extract the desired *agrB* and *agrD*, corresponding to the *agr* BGC, the PF04647 and TIGR04223 domains were used as search queries, respectively. Specifically, all open reading frames (ORFs) encoding AIP BGCs in each genome were annotated using prodigal-short (*68*). Subsequently, small ORFs (≤120 amino acids) containing start/stop codons and ribosome-binding site motifs were then analyzed by TrRiPP (default parameters) to identify RiPP precursors.

The SSN analysis of AgrDs was conducted using the EFI-EST tool (*69*). Sequences exhibiting greater than 50% similarity were grouped into distinct families. Only those families containing more than 25 sequences were selected for co-occurrence analysis with BGCs, which encompassed a total of 16,501 genomes. After extracting the antiSMASH results for these genomes, BGCs associated with "auto_inducing_peptide" were excluded. The BiG-SLiCE tool (*70*) was then used to cluster the remaining BGCs based on a distance threshold of 0.2. The co-occurrence ratio was calculated as the number of sequences in family that co-occurred with cluster, divided by the total number of sequences in family. Last, the SSN and co-occurrence network were visualized using Cytoscape (*71*).

Supplementary Materials

The PDF file includes:

Figs. S1 to S27
Tables S1 to S8
Legends for data S1 to S6
References

Other Supplementary Material for this manuscript includes the following:

Data S1 to S6

REFERENCES AND NOTES

1. W. C. Fuqua, S. C. Winans, E. P. Greenberg, Quorum sensing in bacteria: The LuxR-LuxI family of cell density-responsive transcriptional regulators. *J. Bacteriol.* **176**, 269–275 (1994).
2. M. Whiteley, S. P. Diggle, E. P. Greenberg, Progress in and promise of bacterial quorum sensing research. *Nature* **551**, 313–320 (2017).
3. M. J. Eickhoff, B. L. Bassler, SnapShot: Bacterial quorum sensing. *Cell* **174**, 1328–1328.e1 (2018).
4. R. A. Oliveira, V. Cabral, I. Torcato, K. B. Xavier, Deciphering the quorum-sensing lexicon of the gut microbiota. *Cell Host Microbe* **31**, 500–512 (2023).
5. K. Papenfort, B. L. Bassler, Quorum sensing signal–response systems in Gram-negative bacteria. *Nat. Rev. Microbiol.* **14**, 576–588 (2016).
6. A. M. Stevens, Y. Queneau, L. Soulère, S. von Bodman, A. Doutheau, Mechanisms and synthetic modulators of AHL-dependent gene regulation. *Chem. Rev.* **111**, 4–27 (2011).
7. A. Vendeville, K. Winzer, K. Heurlier, C. M. Tang, K. R. Hardie, Making "sense" of metabolism: Autoinducer-2, LUXS and pathogenic bacteria. *Nat. Rev. Microbiol.* **3**, 383–396 (2005).
8. J. D. Rudolf, S. Loesgen, Pyrazinone biosynthesis and signaling—Myxo style. *ACS Cent. Sci.* **10**, 511–513 (2024).
9. C. S. Kim, A. Gatsios, S. Cuesta, Y. C. Lam, Z. Wei, H. Chen, R. M. Russell, E. E. Shine, R. Wang, T. P. Wyche, G. Piizzi, R. A. Flavell, N. W. Palm, V. Sperandio, J. M. Crawford, Characterization of autoinducer-3 structure and biosynthesis in *E. coli*. *ACS Cent. Sci.* **6**, 197–206 (2020).
10. M. B. Neiditch, G. C. Capodagli, G. Prehna, M. J. Federle, Genetic and structural analyses of RRNPP intercellular peptide signaling of gram-positive bacteria. *Annu. Rev. Genet.* **51**, 311–333 (2017).
11. M. Thoendel, J. S. Kavanaugh, C. E. Flack, A. R. Horswill, Peptide signaling in the *Staphylococci*. *Chem. Rev.* **111**, 117–151 (2011).
12. S. Mukherjee, B. L. Bassler, Bacterial quorum sensing in complex and dynamically changing environments. *Nat. Rev. Microbiol.* **17**, 371–382 (2019).
13. S. Azimi, A. D. Klementiev, M. Whiteley, S. P. Diggle, Bacterial quorum sensing during infection. *Annu. Rev. Microbiol.* **74**, 201–219 (2020).
14. P. V. Bramhachari, "Novel insights on the functional aspects of quorum sensing systems and its applications in medicine, food industry, and agriculture" in *Implication of Quorum Sensing and Biofilm Formation in Medicine, Agriculture and Food Industry*, P. V. Bramhachari, Ed. (Springer, 2019), pp. 3–10.
15. B. Wang, T. W. Muir, Regulation of virulence in *Staphylococcus aureus*: Molecular mechanisms and remaining puzzles. *Cell Chemical Biology* **23**, 214–224 (2016).
16. G. Ji, R. Beavis, R. P. Novick, Bacterial interference caused by autoinducing peptide variants. *Science* **276**, 2027–2030 (1997).
17. U. K. B. Ahmed, J. D. Ballard, Autoinducing peptide-based quorum signaling systems in *Clostridioides difficile*. *Curr. Opin. Microbiol.* **65**, 81–86 (2022).
18. E. M. Molloy, M. Dell, V. G. Hänsch, K. L. Dunbar, R. Feldmann, A. Oberheide, L. Seyfarth, J. Kumpfmüller, T. Horch, H.-D. Arndt, C. Hertweck, Enzyme-primed native chemical ligation produces autoinducing cyclopeptides in *Clostridia*. *Angew. Chem. Int. Ed. Engl.* **60**, 10670–10679 (2021).
19. M. E. Olson, D. A. Todd, C. R. Schaeffer, A. E. Paharik, M. J. Van Dyke, H. Büttner, P. M. Dunman, H. Rohde, N. B. Cech, P. D. Fey, A. R. Horswill, *Staphylococcus epidermidis agr* quorum-sensing system: Signal identification, cross talk, and importance in colonization. *J. Bacteriol.* **196**, 3482–3493 (2014).
20. B. H. Gless, M. S. Bojer, P. Peng, M. Baldry, H. Ingmer, C. A. Olsen, Identification of autoinducing thiodepsipeptides from staphylococci enabled by native chemical ligation. *Nat. Chem.* **11**, 463–469 (2019).
21. A. E. Paharik, C. P. Parlet, N. Chung, D. A. Todd, E. I. Rodriguez, M. J. Van Dyke, N. B. Cech, A. R. Horswill, Coagulase-negative staphylococcal strain prevents *Staphylococcus aureus* colonization and skin infection by blocking quorum sensing. *Cell Host Microbe* **22**, 746–756.e5 (2017).

22. B. H. Gless, B. S. Bejder, L. Vitolo, L. Marques, P. S. Andersen, M. S. Bojer, H. Ingmer, C. A. Olsen, Chemical phylogenetics of the staphylococcal quorum sensing landscape. bioRxiv 440348 [Preprint] (2021). https://doi.org/10.1101/2021.04.18.440348.
23. A. Lareen, F. Burton, P. Schäfer, Plant root-microbe communication in shaping root microbiomes. *Plant Mol. Biol.* **90**, 575–587 (2016).
24. S. Beirinckx, T. Viaene, A. Haegeman, J. Debode, F. Amery, S. Vandenabeele, H. Nelissen, D. Inzé, R. Tito, J. Raes, C. De Tender, S. Goormachtig, Tapping into the maize root microbiome to identify bacteria that promote growth under chilling conditions. *Microbiome* **8**, 54 (2020).
25. L. Philippot, J. M. Raaijmakers, P. Lemanceau, W. H. van der Putten, Going back to the roots: The microbial ecology of the rhizosphere. *Nat. Rev. Microbiol.* **11**, 789–799 (2013).
26. N. Chen, P. Cai, D. Zhang, J. Zhang, Z. Zhong, Y.-X. Li, Metabolic engineering of "last-line antibiotic" colistin in *Paenibacillus polymyxa*. *Metab. Eng.* **85**, 35–45 (2024).
27. E. N. Grady, J. MacDonald, L. Liu, A. Richman, Z.-C. Yuan, Current knowledge and perspectives of *Paenibacillus*: A review. *Microb. Cell Fact.* **15**, 203 (2016).
28. R. Choong-Min, K. Jinwoo, C. Okhee, P. Soo-Young, P. Seung-Hwan, P. Chang-Seuk, Nature of a root-associated Paenibacillus polymyxa from field-grown winter barley in Korea. *J. Microbiol. Biotechnol.* **15**, 984–991 (2005).
29. H. Jeong, S.-K. Choi, C.-M. Ryu, S.-H. Park, Chronicle of a soil bacterium: *Paenibacillus polymyxa* E681 as a tiny guardian of plant and human health. *Front. Microbiol.* **10**, 467 (2019).
30. P. Cai, J. He, Z.-M. Song, Y. Tian, Z. Zhong, D. Zhang, Y. Shi, X. Tang, Y.-X. Li, Uncovering untapped carboxylic acid reductases (CARs) for one-step biosynthesis and diversification of bioactive nitrogen-containing heterocycles. *ACS Catal.* **13**, 15404–15416 (2023).
31. E. Li, K. Liu, S. Yang, L. Li, K. Ran, X. Sun, J. Qu, L. Zhao, Y. Xin, F. Zhu, J. Ma, F. Song, Z. Li, Analysis of the complete genome sequence of *Paenibacillus sp*. lzh-N1 reveals its antagonistic ability. *BMC Genomics* **25**, 276 (2024).
32. D. Hyatt, G.-L. Chen, P. F. LoCascio, M. L. Land, F. W. Larimer, L. J. Hauser, Prodigal: Prokaryotic gene recognition and translation initiation site identification. *BMC Bioinformatics* **11**, 119 (2010).
33. Z. Cheng, B.-B. He, K. Lei, Y. Gao, Y. Shi, Z. Zhong, H. Liu, R. Liu, H. Zhang, S. Wu, W. Zhang, X. Tang, Y.-X. Li, Rule-based omics mining reveals antimicrobial macrocyclic peptides against drug-resistant clinical isolates. *Nat. Commun.* **15**, 4901 (2024).
34. S. Langendries, S. Goormachtig, *Paenibacillus polymyxa*, a Jack of all trades. *Environ. Microbiol.* **23**, 5659–5669 (2021).
35. A. Boo, T. Toth, Q. Yu, A. Pfotenhauer, B. D. Fields, S. C. Lenaghan, C. N. Stewart, C. A. Voigt, Synthetic microbe-to-plant communication channels. *Nat Commun.* **15**, 1817 (2024).
36. Z. Wang, Z. Li, Y. Zhang, J. Liao, K. Guan, J. Zhai, P. Meng, X. Tang, T. Dong, Y. Song, Root hair developmental regulators orchestrate drought triggered microbiome changes and the interaction with beneficial Rhizobiaceae. *Nat. Commun.* **15**, 10068 (2024).
37. Y. Gao, Z. Zhong, D. Zhang, J. Zhang, Y.-X. Li, Exploring the roles of ribosomal peptides in prokaryote-phage interactions through deep learning-enabled metagenome mining. *Microbiome* **12**, 94 (2024).
38. R. J. Dubos, Studies on a bactericidal agent extracted from a soil bacillus: I. Preparation of the agent. Its activity in vitro. *J. Exp. Med.* **70**, 1–10 (1939).
39. D. Konz, S. Doekel, M. A. Marahiel, Molecular and biochemical characterization of the protein template controlling biosynthesis of the lipopeptide lichenysin. *J. Bacteriol.* **181**, 133–140 (1999).
40. J. Vater, B. Niu, K. Dietel, R. Borriss, Characterization of novel fusaricidins produced by *Paenibacillus polymyxa*-M1 using MALDI-TOF mass spectrometry. *J. Am. Soc. Mass Spectrom.* **26**, 1548–1558 (2015).
41. M. Jangra, M. Kaur, H. Nandanwar, In-vitro studies on a natural lantibiotic, paenibacillin: A new-generation antibacterial drug candidate to overcome multi-drug resistance. *Int. J. Antimicrob. Agents* **53**, 838–843 (2019).
42. J.-E. Park, H.-R. Kim, S.-Y. Park, S.-K. Choi, S.-H. Park, Identification of the biosynthesis gene cluster for the novel lantibiotic paenilan from Paenibacillus polymyxa E681 and characterization of its product. *J. Appl. Microbiol.* **123**, 1133–1147 (2017).
43. S. A. Cochrane, B. Findlay, A. Bakhtiary, J. Z. Acedo, E. M. Rodriguez-Lopez, P. Mercier, J. C. Vederas, Antimicrobial lipopeptide tridecaptin A1 selectively binds to Gram-negative lipid II. *Proc. Natl. Acad. Sci. U.S.A.* **113**, 11561–11566 (2016).
44. Y. Tal-Gan, M. Ivancic, G. Cornilescu, H. E. Blackwell, Characterization of structural elements in native autoinducing peptides and non-native analogues that permit the differential modulation of AgrC-type quorum sensing receptors in *Staphylococcus aureus*. *Org. Biomol. Chem.* **14**, 113–121 (2015).
45. A. Zipperer, M. C. Konnerth, C. Laux, A. Berscheid, D. Janek, C. Weidenmaier, M. Burian, N. A. Schilling, C. Slavetinsky, M. Marschal, M. Willmann, H. Kalbacher, B. Schittek, H. Brötz-Oesterhelt, S. Grond, A. Peschel, B. Krismer, Human commensals producing a novel antibiotic impair pathogen colonization. *Nature* **535**, 511–516 (2016).
46. A. Wuster, M. M. Babu, Conservation and evolutionary dynamics of the *agr* cell-to-cell communication system across firmicutes. *J. Bacteriol.* **190**, 743–746 (2008).
47. B. S. Bejder, F. Monda, B. H. Gless, M. S. Bojer, H. Ingmer, C. A. Olsen, A short-lived peptide signal regulates cell-to-cell communication in Listeria monocytogenes. bioRxiv 547616 [Preprint] (2023). https://doi.org/10.1101/2023.07.04.547616.
48. T. F. C. Chin-A-Woeng, D. van den Broek, G. de Voer, K. M. G. M. van der Drift, S. Tuinman, J. E. Thomas-Oates, B. J. J. Lugtenberg, G. V. Bloemberg, Phenazine-1-carboxamide production in the biocontrol strain *Pseudomonas chlororaphis* PCL1391 is regulated by multiple factors secreted into the growth medium. *Mol. Plant Microbe Interact.* **14**, 969–979 (2001).
49. J. Jung, K. O. Yu, A. B. Ramzi, S. H. Choe, S. W. Kim, S. O. Han, Improvement of surfactin production in *Bacillus subtilis* using synthetic wastewater by overexpression of specific extracellular signaling peptides, comX and phrC. *Biotechnol. Bioeng.* **109**, 2349–2356 (2012).
50. K. B. Schneider, T. M. Palmer, A. D. Grossman, Characterization of comQ and comX, two genes required for production of ComX pheromone in *Bacillus subtilis*. *J. Bacteriol.* **184**, 410–419 (2002).
51. C. Jenul, S. Sieber, C. Daeppen, A. Mathew, M. Lardi, G. Pessi, D. Hoepfner, M. Neuburger, A. Linden, K. Gademann, L. Eberl, Biosynthesis of fragin is controlled by a novel quorum sensing signal. *Nat. Commun.* **9**, 1297 (2018).
52. A. Eliasson Lantz, P. Jørgensen, E. Poulsen, C. Lindemann, L. Olsson, Determination of cell mass and polymyxin using multi-wavelength fluorescence. *J. Biotechnol.* **121**, 544–554 (2006).
53. T. Claridge, Software review of MNova: NMR data processing, analysis, and prediction software. *J. Chem. Inf. Model.* **49**, 1136–1137 (2009).
54. J. Altenbuchner, Editing of the *Bacillus subtilis* genome by the CRISPR-Cas9 system. *Appl. Environ. Microbiol.* **82**, 5421–5427 (2016).
55. M. A. Konkol, K. M. Blair, D. B. Kearns, Plasmid-encoded ComI inhibits competence in the ancestral 3610 strain of *Bacillus subtilis*. *J. Bacteriol.* **195**, 4085–4093 (2013).
56. B. H. Gless, P. Peng, K. D. Pedersen, C. H. Gotfredsen, H. Ingmer, C. A. Olsen, Structure–activity relationship study based on autoinducing peptide (AIP) from dog pathogen *S. schleiferi*. *Org. Lett.* **19**, 5276–5279 (2017).
57. S. Chen, Y. Zhou, Y. Chen, J. Gu, fastp: An ultra-fast all-in-one FASTQ preprocessor. *Bioinformatics* **34**, i884–i890 (2018).
58. B. Langmead, S. L. Salzberg, Fast gapped-read alignment with Bowtie 2. *Nat. Methods* **9**, 357–359 (2012).
59. Y. Liao, G. K. Smyth, W. Shi, featureCounts: An efficient general purpose program for assigning sequence reads to genomic features. *Bioinformatics* **30**, 923–930 (2014).
60. D. E. Wood, J. Lu, B. Langmead, Improved metagenomic analysis with Kraken 2. *Genome Biol.* **20**, 257 (2019).
61. J. Lu, F. P. Breitwieser, P. Thielen, S. L. Salzberg, Bracken: Estimating species abundance in metagenomics data. *PeerJ Comput. Sci.* **3**, e104 (2017).
62. J. Zhang, Y.-X. Liu, X. Guo, Y. Qin, R. Garrido-Oter, P. Schulze-Lefert, Y. Bai, High-throughput cultivation and identification of bacteria from the plant root microbiota. *Nat. Protoc.* **16**, 988–1012 (2021).
63. K. Katoh, D. M. Standley, MAFFT multiple sequence alignment software version 7: Improvements in performance and usability. *Mol. Biol. Evol.* **30**, 772–780 (2013).
64. S. Capella-Gutiérrez, J. M. Silla-Martínez, T. Gabaldón, trimAl: A tool for automated alignment trimming in large-scale phylogenetic analyses. *Bioinformatics* **25**, 1972–1973 (2009).
65. M. N. Price, P. S. Dehal, A. P. Arkin, FastTree 2 – Approximately maximum-likelihood trees for large alignments. *PLOS ONE* **5**, e9490 (2010).
66. I. Letunic, P. Bork, Interactive Tree of Life (iTOL) v6: Recent updates to the phylogenetic tree display and annotation tool. *Nucleic Acids Res.* **52**, W78–W82 (2024).
67. K. Blin, S. Shaw, A. M. Kloosterman, Z. Charlop-Powers, G. P. van Wezel, M. H. Medema, T. Weber, antiSMASH 6.0: Improving cluster detection and comparison capabilities. *Nucleic Acids Res.* **49**, W29–W35 (2021).
68. J. Santos-Aberturas, G. Chandra, L. Frattaruolo, R. Lacret, T. H. Pham, N. M. Vior, T. H. Eyles, A. W. Truman, Uncovering the unexplored diversity of thioamidated ribosomal peptides in Actinobacteria using the RiPPER genome mining tool. *Nucleic Acids Res.* **47**, 4624–4637 (2019).
69. R. Zallot, N. Oberg, J. A. Gerlt, The EFI web resource for genomic enzymology tools: Leveraging protein, genome, and metagenome databases to discover novel enzymes and metabolic pathways. *Biochemistry* **58**, 4169–4182 (2019).
70. S. A. Kautsar, J. J. J. van der Hooft, D. de Ridder, M. H. Medema, BiG-SLiCE: A highly scalable tool maps the diversity of 1.2 million biosynthetic gene clusters. *Gigascience* **10**, giaa154 (2021).
71. P. Shannon, A. Markiel, O. Ozier, N. S. Baliga, J. T. Wang, D. Ramage, N. Amin, B. Schwikowski, T. Ideker, Cytoscape: A software environment for integrated models of biomolecular interaction networks. *Genome Res.* **13**, 2498–2504 (2003).
72. C. Vuong, C. Gerke, G. A. Somerville, E. R. Fischer, M. Otto, Quorum-sensing control of biofilm factors in *Staphylococcus epidermidis*. *J Infect Dis* **188**, 706–718 (2003).
73. M. M. Brown, J. M. Kwiecinski, L. M. Cruz, A. Shahbandi, D. A. Todd, N. B. Cech, A. R. Horswill, Novel peptide from commensal *Staphylococcus simulans* blocks methicillin-resistant *Staphylococcus aureus* quorum sensing and protects host skin from damage. *Antimicrob. Agents Chemother.* **64**, e00172-20 (2020).

74. M. R. Williams, S. K. Costa, L. S. Zaramela, S. Khalil, D. A. Todd, H. L. Winter, J. A. Sanford, A. M. O'Neill, M. C. Liggins, T. Nakatsuji, N. B. Cech, A. L. Cheung, K. Zengler, A. R. Horswill, R. L. Gallo, Quorum sensing between bacterial species on the skin protects against epidermal injury in atopic dermatitis. *Sci. Transl. Med.* **11**, eaat8329 (2019).
75. M. M. Severn, M. R. Williams, A. Shahbandi, Z. L. Bunch, L. M. Lyon, A. Nguyen, L. S. Zaramela, D. A. Todd, K. Zengler, N. B. Cech, R. L. Gallo, A. R. Horswill, The ubiquitous human skin commensal *Staphylococcus hominis* protects against opportunistic pathogens. *mBio* **13**, e00930–e00922 (2022).
76. M. M. Severn, Y.-S. K. Cho, H. S. Manzer, Z. L. Bunch, A. Shahbandi, D. A. Todd, N. B. Cech, A. R. Horswill, The commensal *Staphylococcus warneri* makes peptide inhibitors of MRSA quorum sensing that protect skin from atopic or necrotic damage. *J. Invest. Dermatol.* **142**, 3349–3352.e5 (2022).
77. M. Kalkum, G. J. Lyon, B. T. Chait, Detection of secreted peptides by using hypothesis-driven multistage mass spectrometry. *Proc. Natl. Acad. Sci. U.S.A.* **100**, 2795–2800 (2003).
78. G. Ji, W. Pei, L. Zhang, R. Qiu, J. Lin, Y. Benito, G. Lina, R. P. Novick, *Staphylococcus intermedius* produces a functional *agr* autoinducing peptide containing a cyclic lactone. *J. Bacteriol.* **187**, 3139–3150 (2005).
79. D. A. Todd, C. P. Parlet, H. A. Crosby, C. L. Malone, K. P. Heilmann, A. R. Horswill, N. B. Cech, Signal biosynthesis inhibition with ambuic acid as a strategy to target antibiotic-resistant infections. *Antimicrob. Agents Chemother.* **61**, e00263-17 (2017).
80. C. U. Riedel, I. R. Monk, P. G. Casey, M. S. Waidmann, C. G. M. Gahan, C. Hill, AgrD-dependent quorum sensing affects biofilm formation, invasion, virulence and global gene expression profiles in *Listeria monocytogenes*. *Mol. Microbiol.* **71**, 1177–1189 (2009).
81. B. S. Bejder, F. Monda, B. H. Gless, M. S. Bojer, H. Ingmer, C. A. Olsen, A short-lived peptide signal regulates cell-to-cell communication in *Listeria monocytogenes*. *Commun. Biol.* **7**, 942 (2024).
82. B. H. Gless, B. S. Bejder, F. Monda, M. S. Bojer, H. Ingmer, C. A. Olsen, Rearrangement of thiodepsipeptides by S → N acyl shift delivers homodetic autoinducing peptides. *J. Am. Chem. Soc.* **143**, 10514–10518 (2021).
83. M. H. Sturme, J. Nakayama, D. Molenaar, Y. Murakami, R. Kunugi, T. Fujii, E. E. Vaughan, M. Kleerebezem, W. M. de Vos, An *agr*-like two-component regulatory system in *Lactobacillus plantarum* is involved in production of a novel cyclic peptide and regulation of adherence. *J. Bacteriol.* **187**, 5224–5235 (2005).
84. J. Nakayama, Y. Cao, T. Horii, S. Sakuda, A. D. L. Akkermans, W. M. De Vos, H. Nagasawa, Gelatinase biosynthesis-activating pheromone: A peptide lactone that mediates a quorum sensing in *Enterococcus faecalis*. *Mol. Microbiol.* **41**, 145–154 (2001).
85. T. J. Verbeke, R. J. Giannone, D. M. Klingeman, N. L. Engle, T. Rydzak, A. M. Guss, T. J. Tschaplinski, S. D. Brown, R. L. Hettich, J. G. Elkins, Pentose sugars inhibit metabolism and increase expression of an AgrD-type cyclic pentapeptide in *Clostridium thermocellum*. *Sci. Rep.* **7**, 43355 (2017).
86. M. Ma, J. Li, B. A. McClane, Structure-function analysis of peptide signaling in the *Clostridium perfringens* Agr-like quorum sensing system. *J. Bacteriol.* **197**, 1807–1818 (2015).
87. E. Steiner, J. Scott, N. P. Minton, K. Winzer, An *agr* quorum sensing system that regulates granulose formation and sporulation in *Clostridium acetobutylicum*. *Appl. Environ. Microbiol.* **78**, 1113–1122 (2012).

Acknowledgments: We thank Y.-M. Eva Fung and J. Yip for help in MS analysis and B. Yan for help in NMR analysis. **Funding:** This work was supported by Research Grants Council of Hong Kong (C7014-24GF, 17115322, and 17102123); National Natural Science Foundation of China (NSFC) General Project (32270286); and Shenzhen Science and Technology Program (RCYX20231211090408015). **Author contributions:** Conceptualization: Y.-X.L., N.C., P.C., and X.L. Methodology: P.C., N.C., X.L., Z.-M.S., and Zewen Li. Investigation: N.C., P.C., X.L., Z.-M.S., J.H., Zhuohan Li, Zewen Li, and D.Z. Visualization: P.C., N.C., X.L., and D.Z. Supervision: Y.-X.L. and Y.S. Writing—original draft: Y.-X.L., N.C., P.C., and X.L. **Competing interests:** The authors declare that they have no competing interests. **Data and materials availability:** All sequencing data generated in this study have been deposited in NCBI SRA with accession number PRJNA1214415. The genome datasets used in this study were collected from NCBI RefSeq database (https://ftp.ncbi.nlm.nih.gov/genomes/refseq/). Codes for this project are available at https://github.com/Linxiaoqianv/Pp-AIP_analysis. Also, it can be accessed in the Zenodo database (https://doi.org/10.5281/zenodo.15051017). The original NMR files of Pp-AIP1 and Pp-AIP2 have been uploaded to The Harvard Dataverse (https://doi.org/10.7910/DVN/JCL7OB). All other data needed to evaluate the conclusions in the paper are present in the paper and/or the Supplementary Materials.

Submitted 10 February 2025
Accepted 19 May 2025
Published 20 June 2025
10.1126/sciadv.adw5076